UCRL-ID-134649

Surface Topographies of One-Year Weight-Loss Coupons of Alloy C-22 from Long-Term Corrosion Testing

Peter J. Bedrossian

June 11, 1999

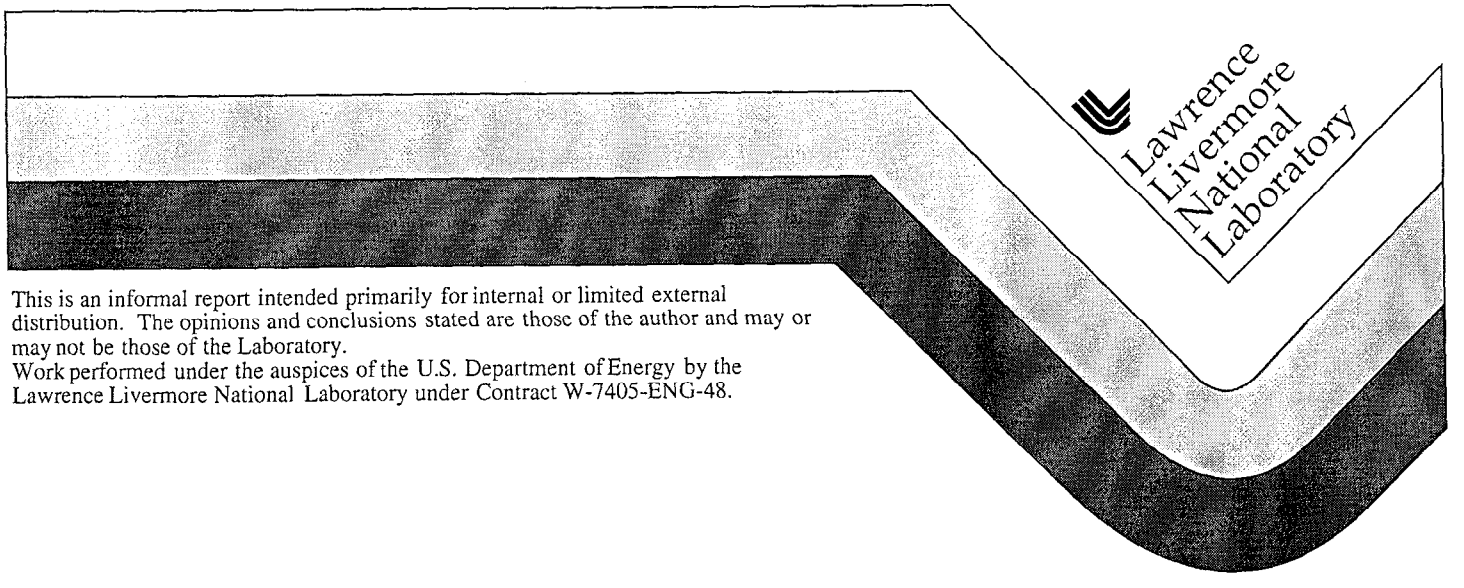

Surface Topographies of One-Year Weight-Loss Coupons of Alloy C-22 from Long-Term Corrosion Testing

Peter J. Bedrossian

Division of Materials Science & Technology
Lawrence Livermore National Laboratory, Livermore CA 94551

11 June 1999

Abstract

We have used an atomic force microscope (AFM) to characterize the surface topographies of weight-loss coupons of Alloy C-22 which had been exposed to two different environments in the Long-Term Corrosion Test Facility at LLNL for one year. We have observed a silicate deposit on these coupons, with the most extensive coverage occuring on the coupon immersed in an acidified bath. We have not detected localized corrosion on these coupons.

Introduction

The Long-Term Corrosion Test Facility (LTCTF) at LLNL is an array of tanks holding various aqueous baths with controlled electrolyte concentrations at 60 or 90°C, in which coupons of candidate materials for the Waste Package are held in either aqueous (below the water line) or vapor (above the water line) phase conditions and removed periodically for analysis. Although the LTCTF coupons have primarly been used for analysis of general corrosion via weight loss, the objective of the present study has been the search for signs of localized corrosion, if any. The "weight loss" coupons are 2 inches long, 1 inch wide, and 1/8 inch thick. Descriptions of the LTCTF and its uses, along with the detailed composition of the aqueous environments, are contained in Reference [1].

The atomic force microscope (AFM), with sub-nanometer vertical resolution, is an ideal tool for detecting pit initiation in localized areas. We have applied AFM to five "weight loss" coupons of Alloy C-22: one control which was never in any bath (DWA163), one aqueous phase sample from an acidified well water, SAW (DWA051), one vapor phase sample from SAW (DWA048), one aqueous phase sample from an alkaline water, SCW (DWA120) and one vapor phase sample from SCW (DWA117). The coupon numbers are official designations of the Yucca Mountain Program (YMP), and the data file numbers correspond to the designations which will be incorporated in the YMP Technical Data Management System. The composition of Alloy C-22 is contained in Reference [2].

Results and Discussion

Representative AFM data are collected and displayed below. Each set of data consists of a large-area scan of at least 25x25 μm followed by smaller-area details of the region

displayed in the large-area scan. We have used a Digital Instruments DM3100 AFM. After the coupons were removed from the LTCTF, they were ultrasonically agitated in deionized water, acetone, and methanol for ten minutes each.

The gross surface topography of the weight-loss coupons is dominated by the machining grooves, with typical heights of several hundred nanometers and typical lateral periodicities of several microns. The machining features on a bare surface are plainly visible on the images of coupon DWA163. Those samples which were removed from the LTCTF exhibit varying degrees of coverage by a deposit on top of this gross topography.

X-ray diffraction scans of all five coupons show that the deposit is predominantly a silicate or SiO_2, with some NaCl appearing on the two samples which were in the SAW tank. The AFM images show that the most extensive coverage of the deposit occured on test coupon DWA051, which was immersed in the SAW bath. The next most extensive coverage occured on test coupon DWA048, which was held above the water line in the SAW bath. The two test coupons removed from the SCW bath showed lesser degrees of coverage by the silicate deposit in both the AFM images and the X-ray diffraction scans.

Incomplete surface coverage by the silicate deposit often results in the appearance of holes in surface, particularly on the DWA051 coupon. We believe that the data collected to date to not show any of these holes extending below the surface of the metal, because the bottoms of the holes are typically flat. One illustration of the analysis leading to this conclusion is shown below in the profile measured along the line trace marked in the image pb990607.023, which spans two such holes. As shown in the profile, the bottoms of the holes are flat, as would be expected for an interruption that occurs only in the silicate deposit.

The following data are presented in this report, with page numbers listed:

Summary

A study of four test coupons of Alloy C-22 removed from the LTCTF after one year showed varying degrees of coverage by silicate deposits but no evidence of localized corrosion by pitting.

Acknowledgments

The author is grateful to David Fix for his extensive AFM data collection, to Dominic Delgiudice for the x-ray measurements, to John Estill and Kenneth King for providing samples from the LTCTF, and to Joseph Farmer, Daniel McCright, and Ronald Musket for helpful discussions. This work was conducted at LLNL under the auspices of the US Department of Energy under Contract W-7405-Eng-48, and was supported by the Yucca Mountain Program.

---

[1] J C Farmer, et al., "Development of Integrated Meghanistically-Based Degradation-Mode Models for Performance Assessment of High-Level Waste Containers," UCRL-ID-130811 (1998), pp. 3 and 49.

[2] L Corb, et al, ed., ASM Handbook, Volume 13: Corrosion. (Metals Park: ASM International, 1987), p. 644.

DWA163 (Control Coupon)

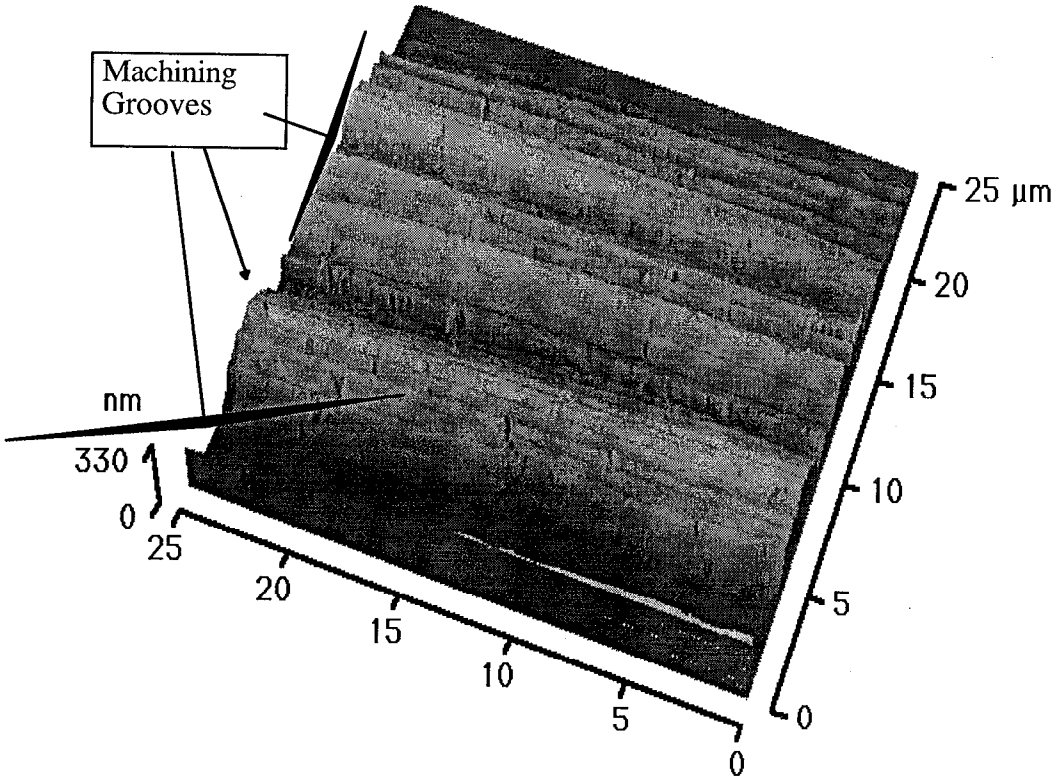

pb990607.019 AFM Image

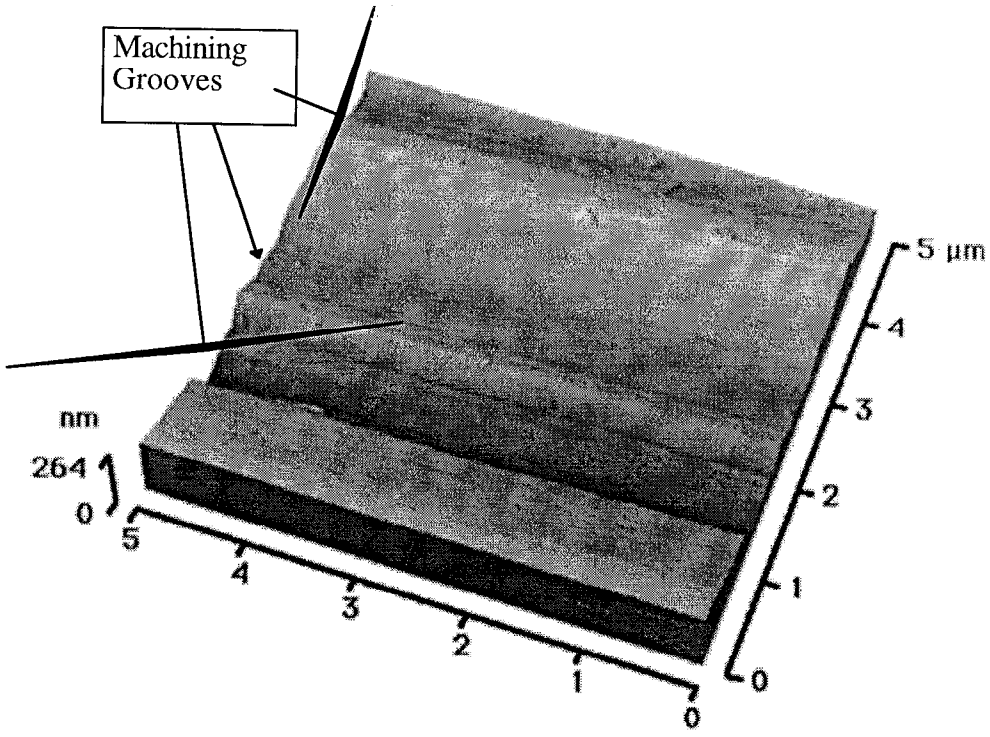

pb990607.020 AFM Image

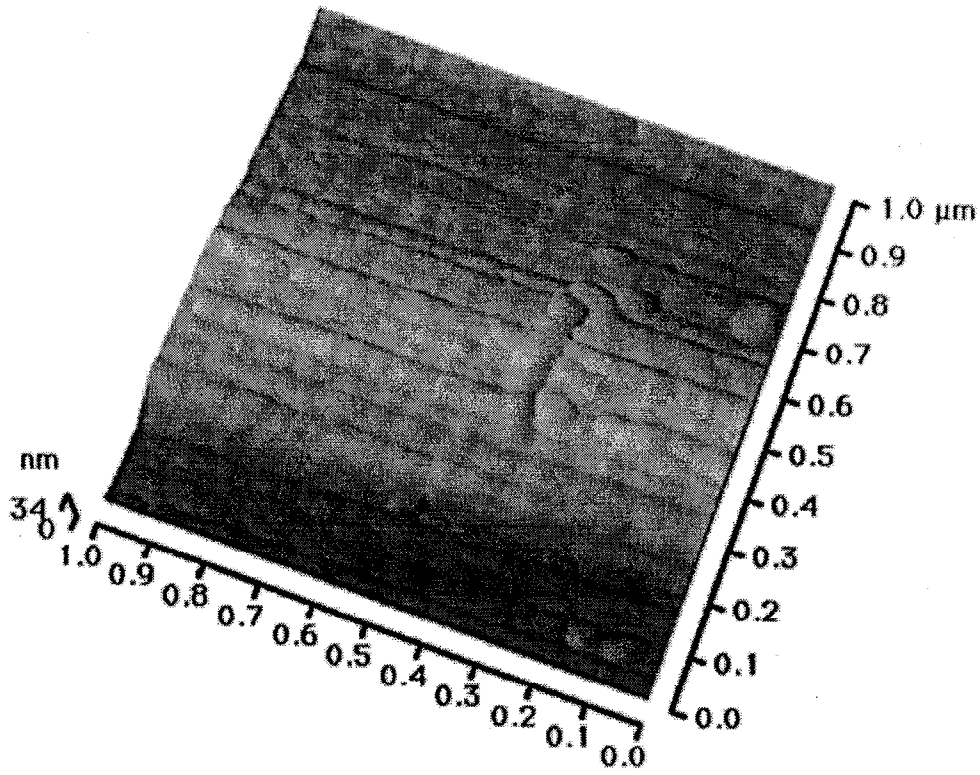

pb990607.021 AFM Image

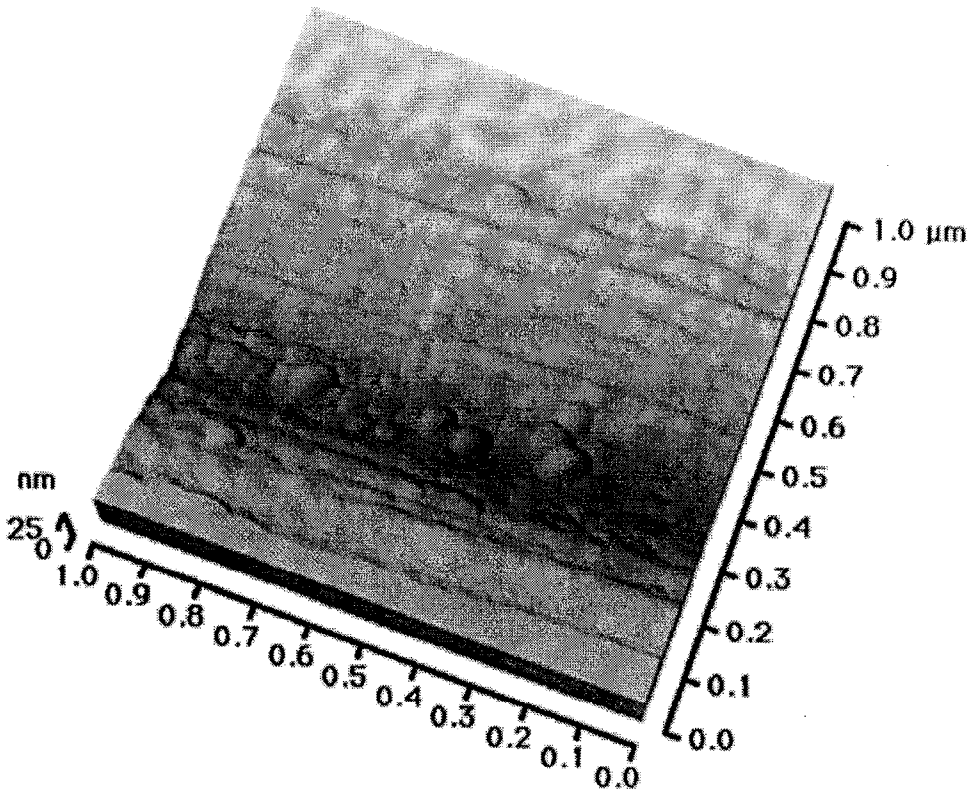

pb990607.022 AFM Image

SAW Test Coupons

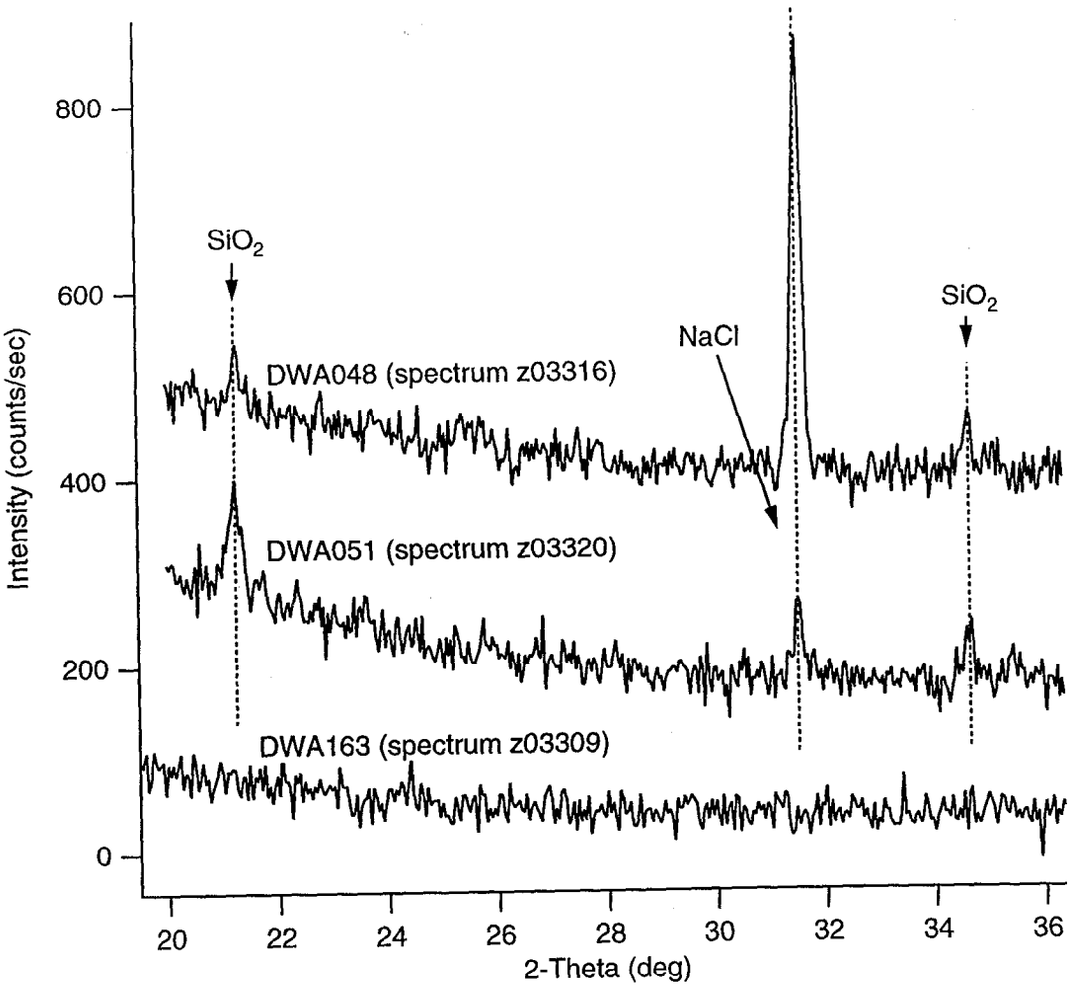

X-Ray Spectra of scales on SAW Coupons

DWA051 (SAW, 90C, Aqueous)

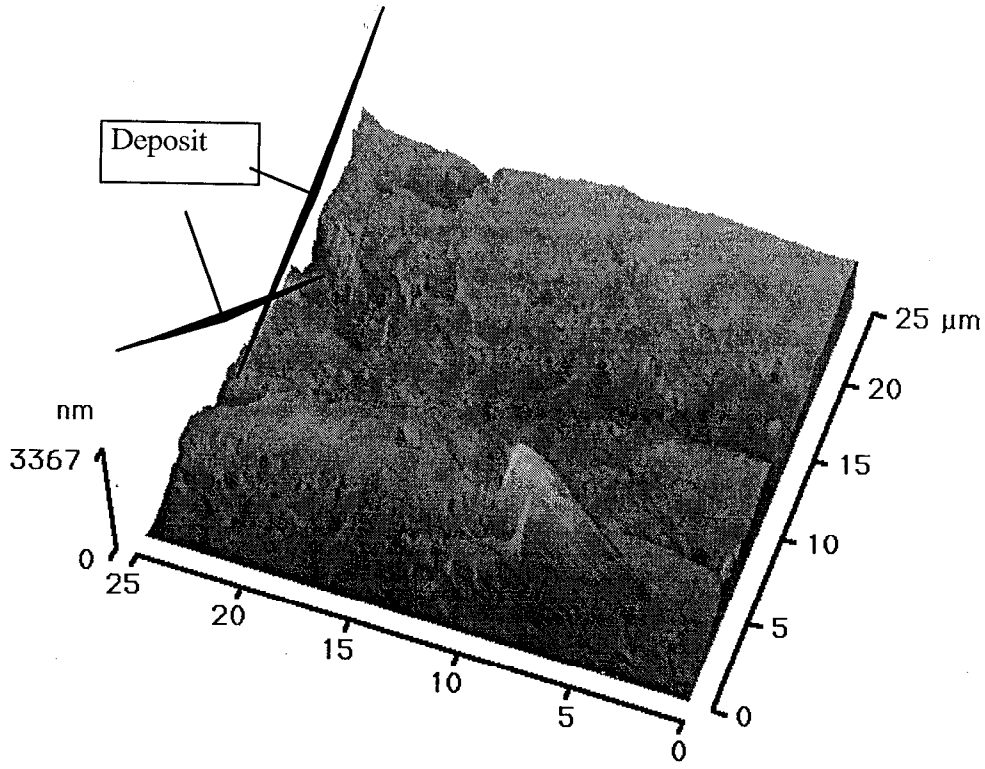

pb990607.023 AFM Image

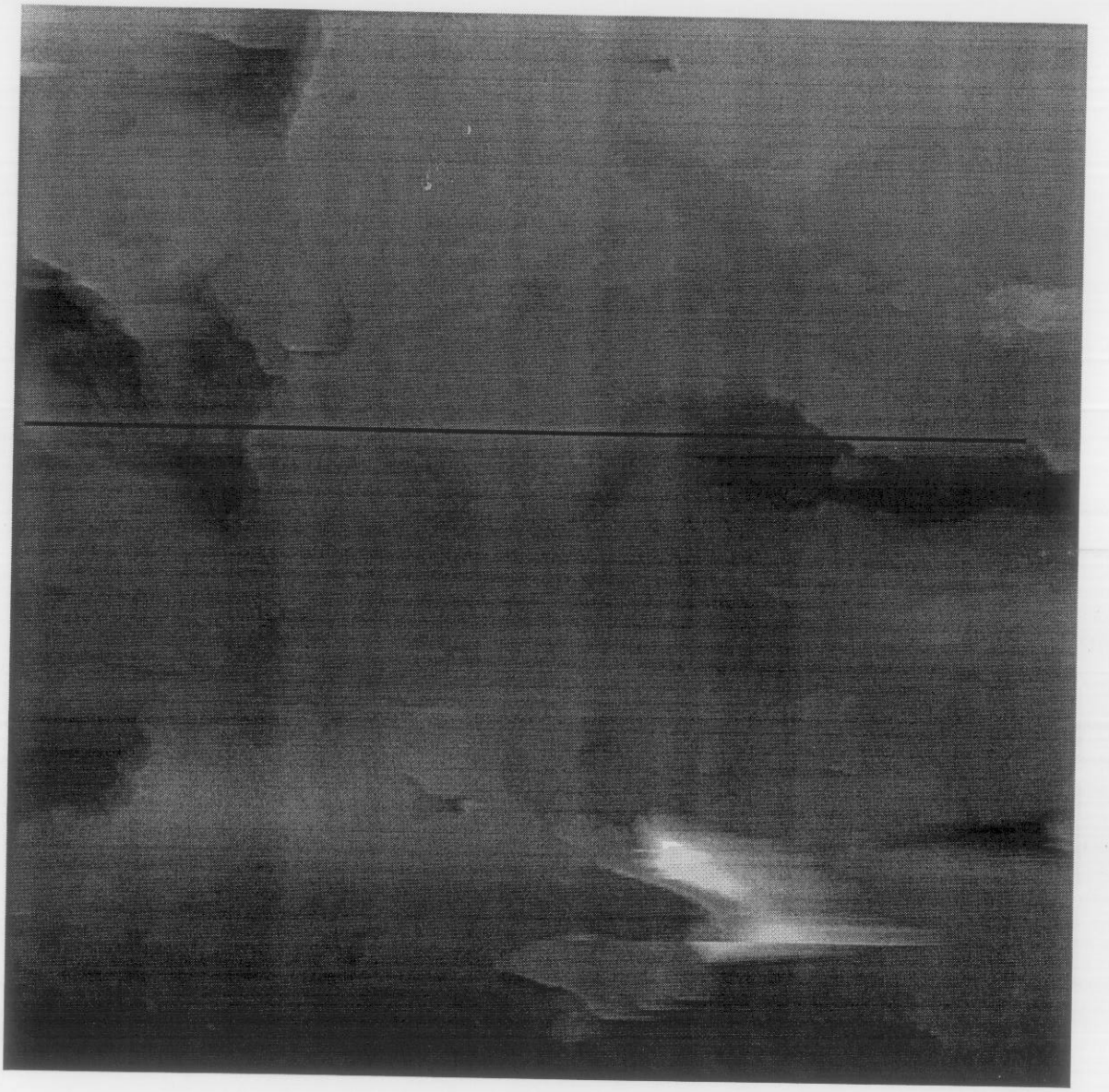

pb990607.023 AFM Image, top view

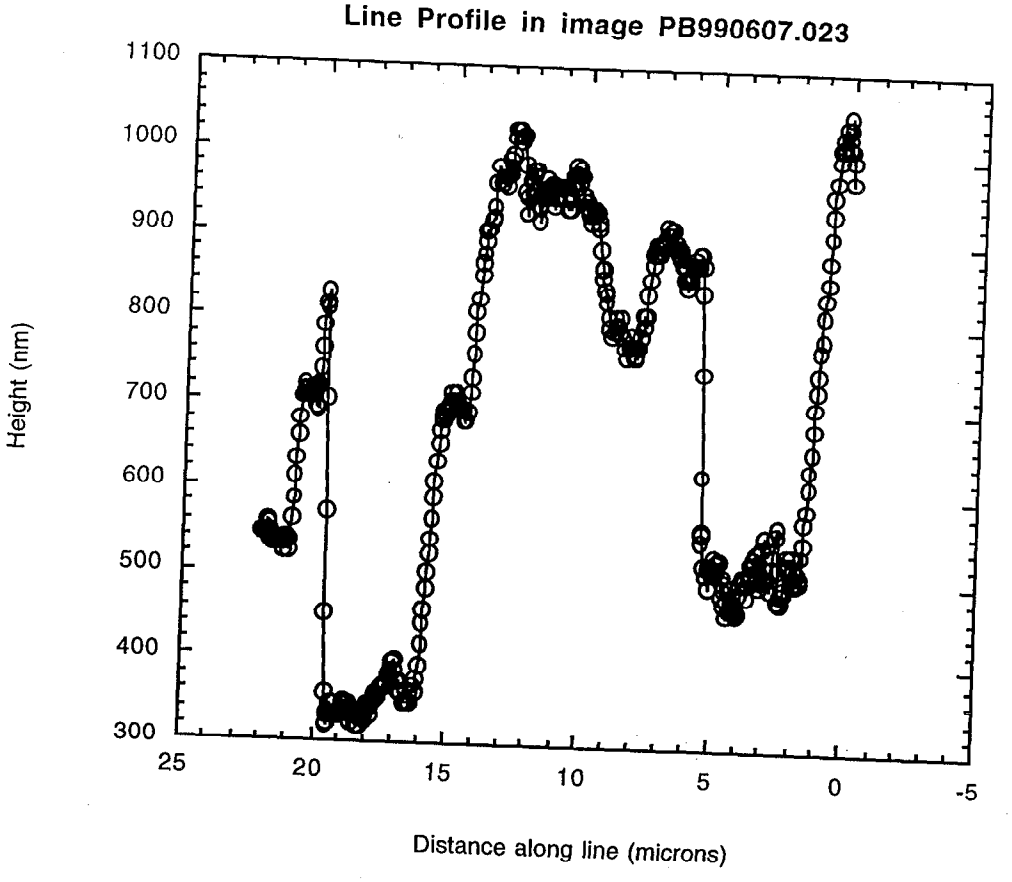

Line Profile in pb990607.023 AFM Image

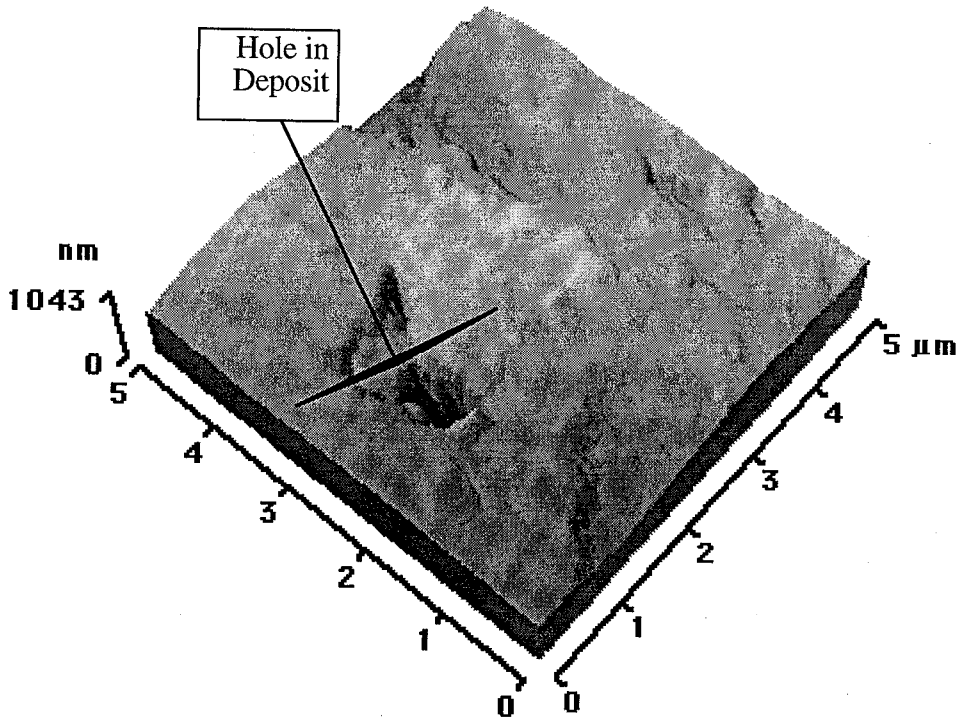

pb990607.024 AFM Image

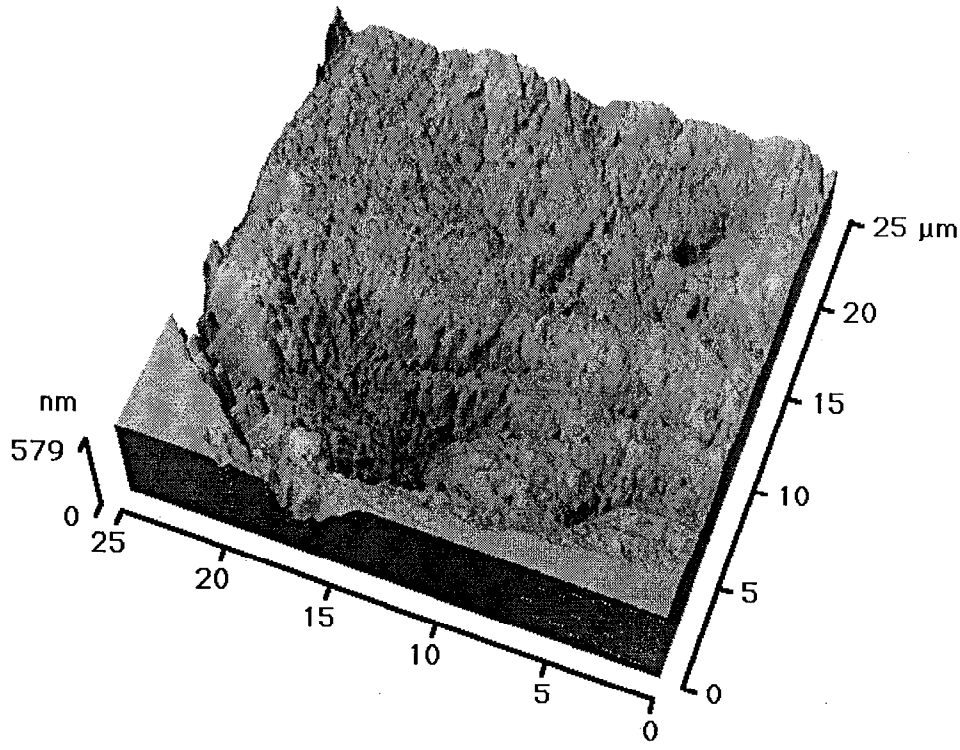

pb990607.025 AFM Image

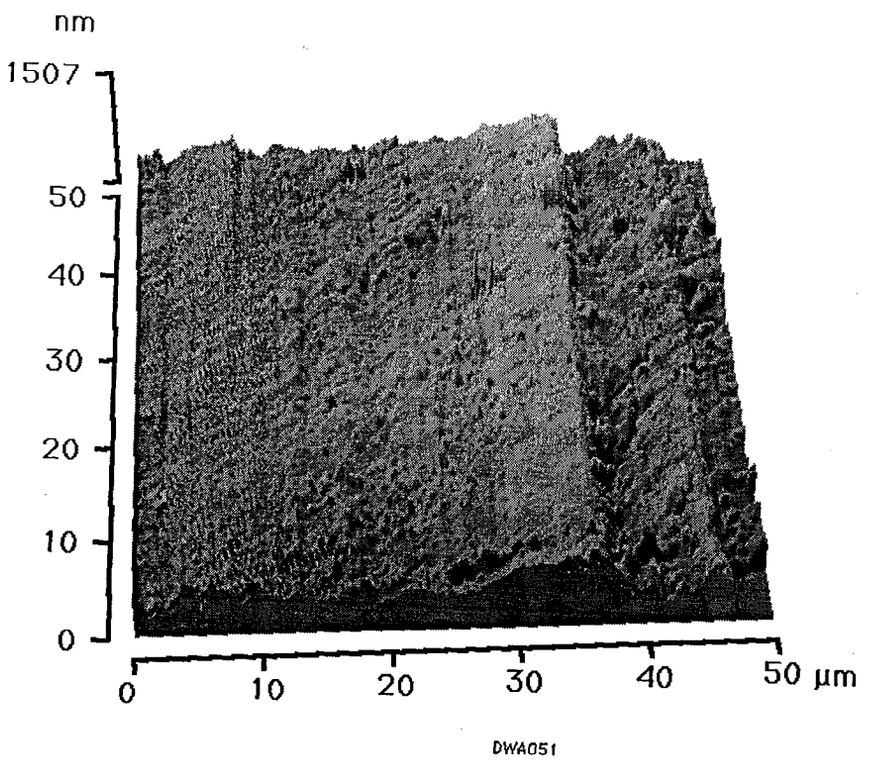

pb990607.033 AFM Image

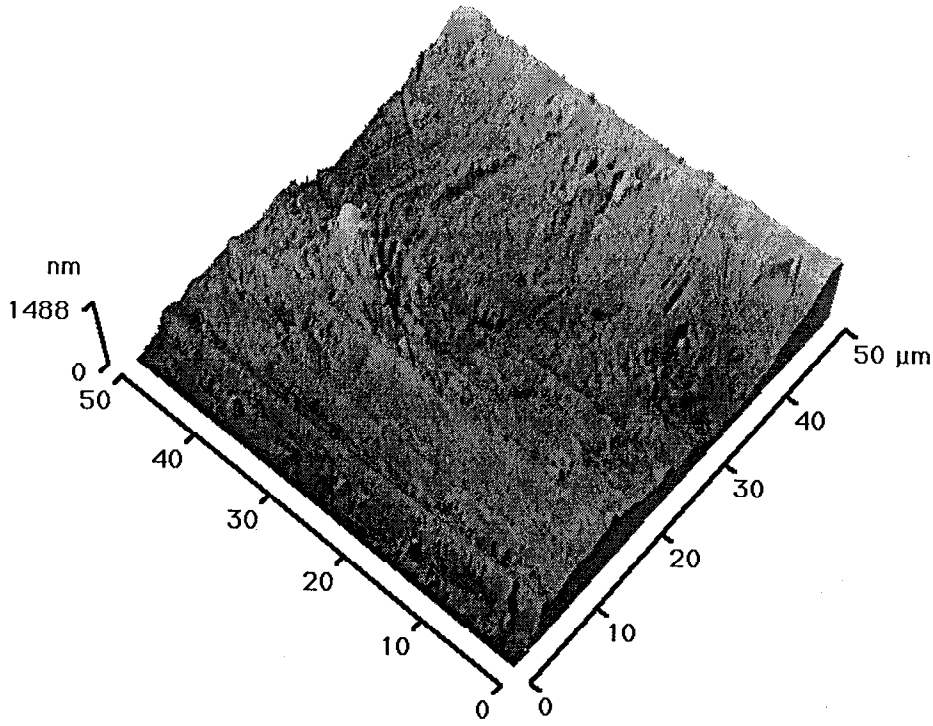

pb990607.029 AFM Image

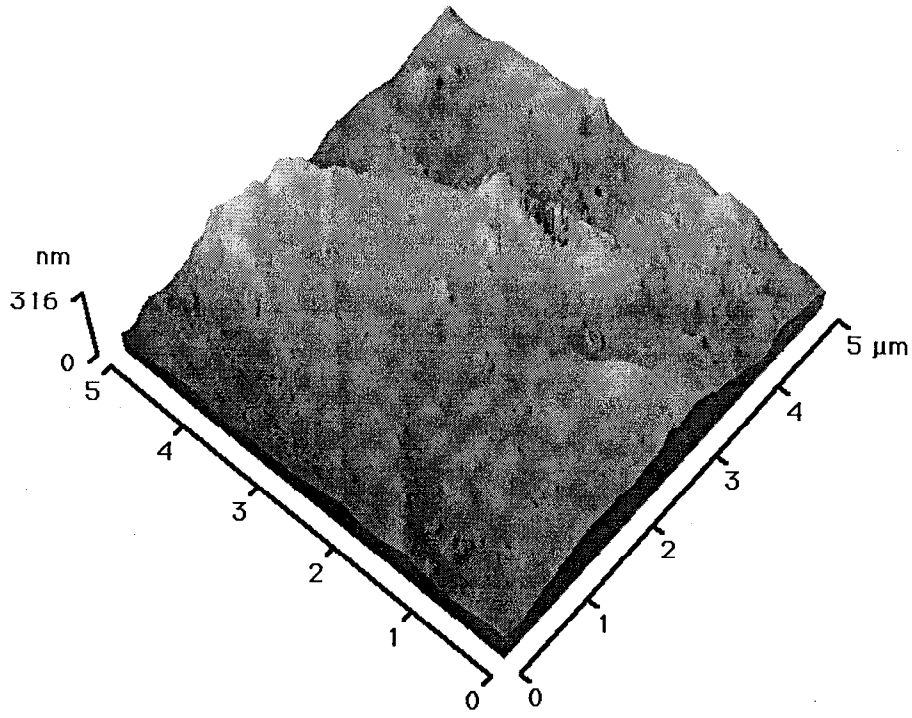

pb990607.030 AFM Image

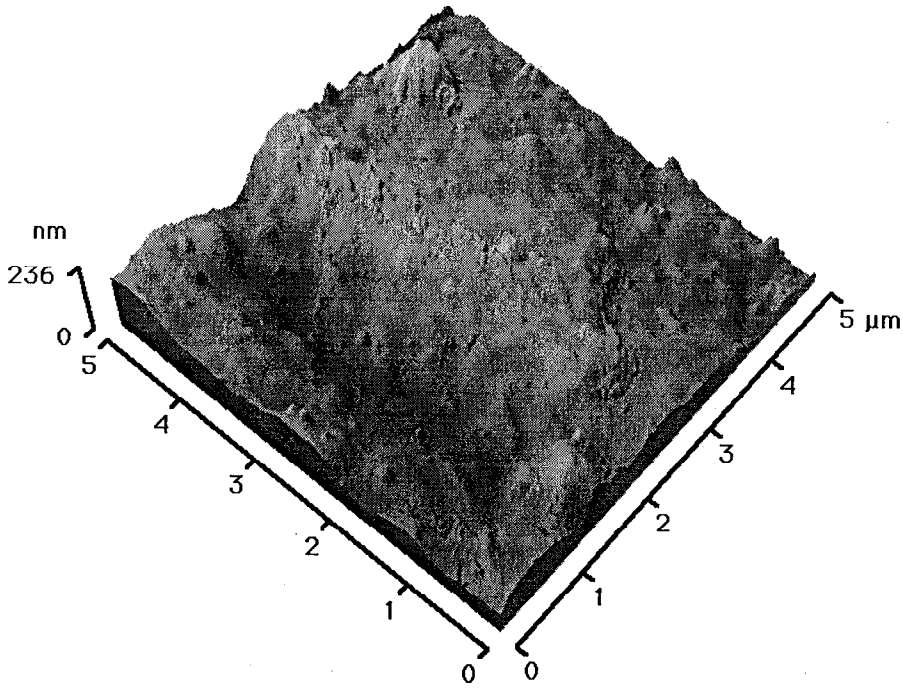

pb990607.031 AFM Image

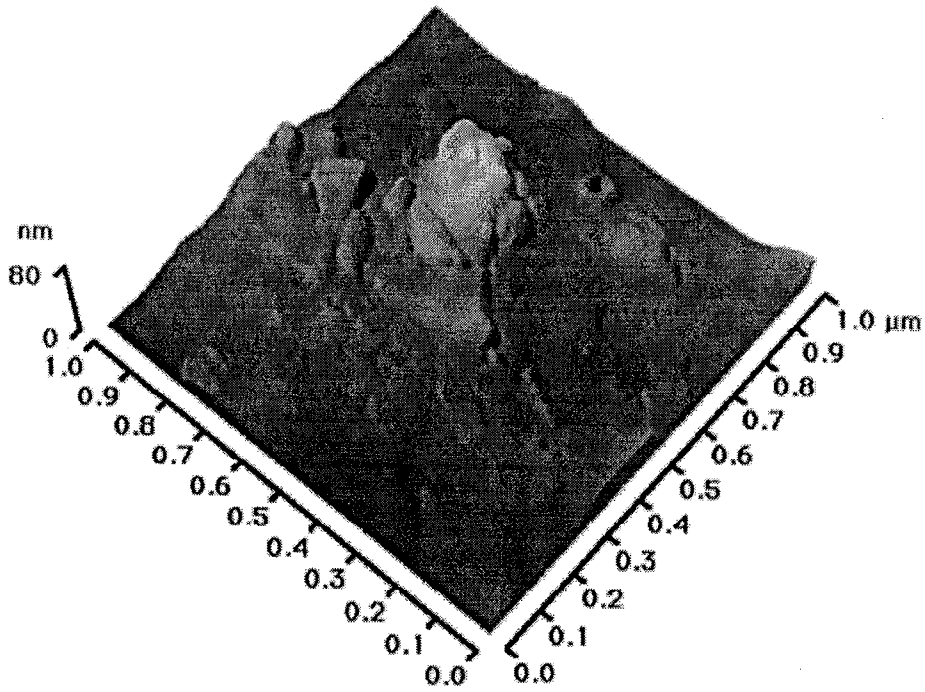

pb990607.032 AFM Image

pb990607.032 AFM Image

DWA048 (SAW, 90C, Vapor)

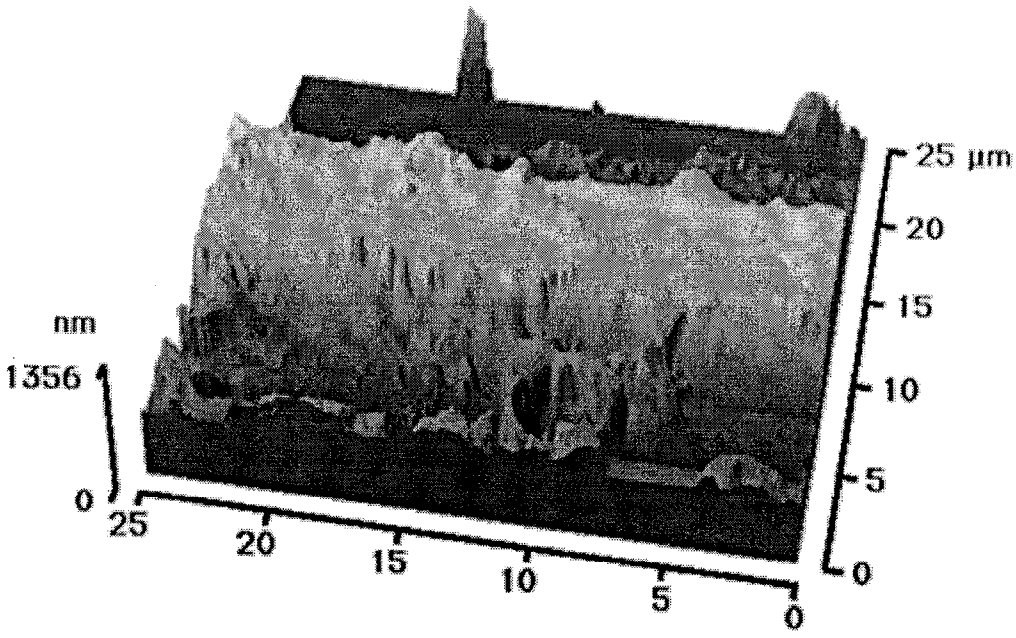

pb990607.046 AFM Image

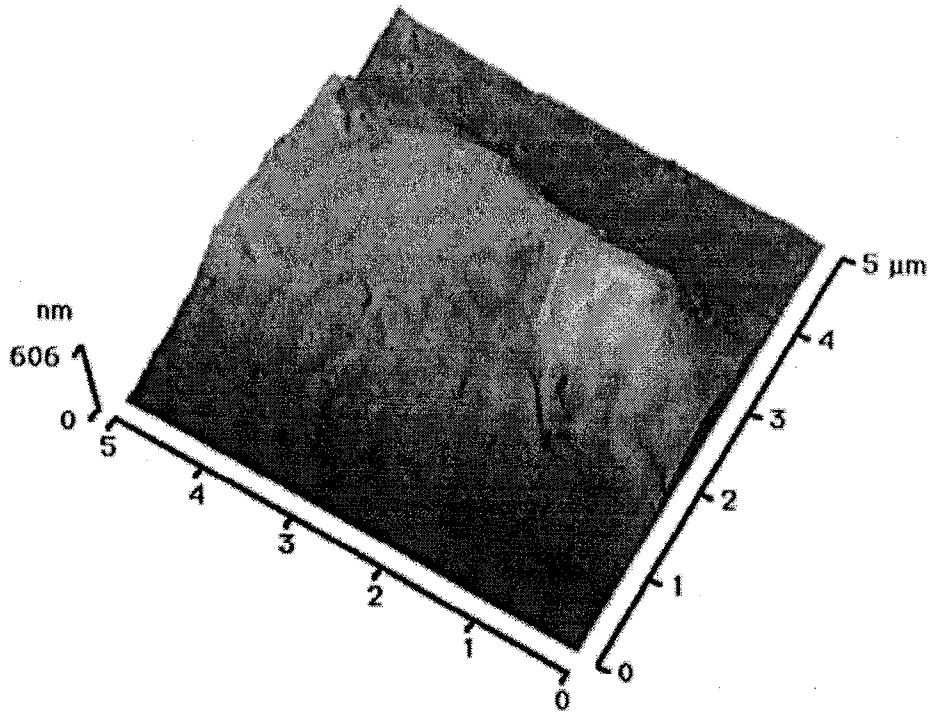

pb990607.045 AFM Image

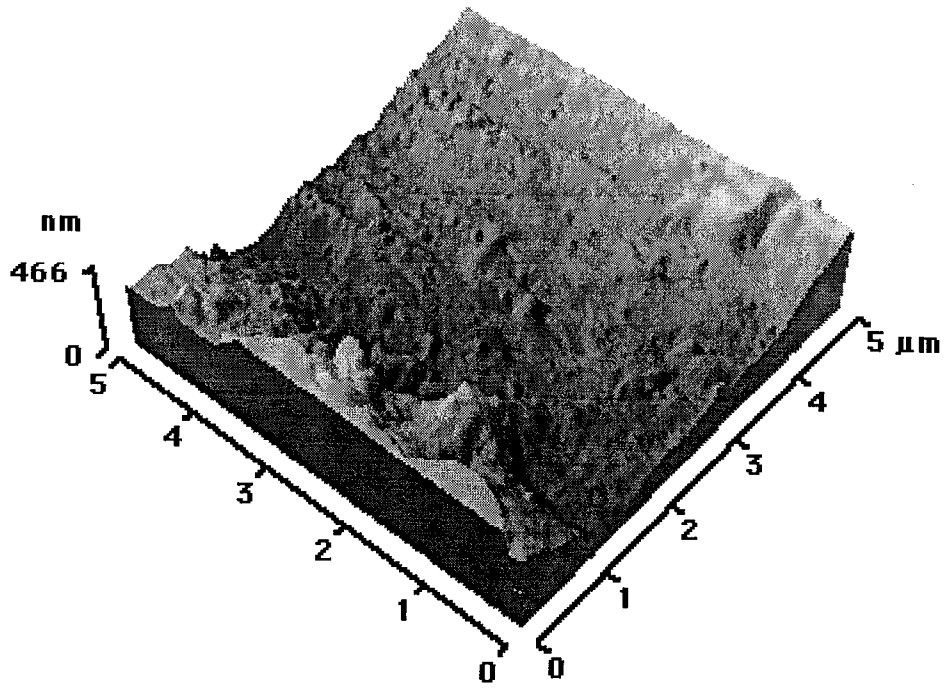

pb990607.048 AFM Image

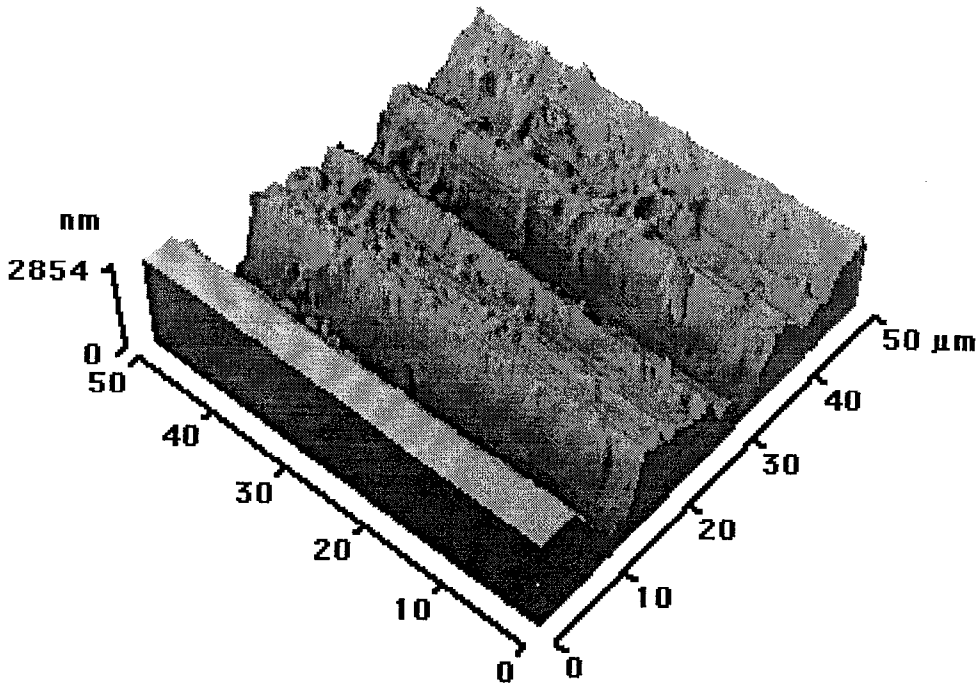

pb990607.050 AFM Image

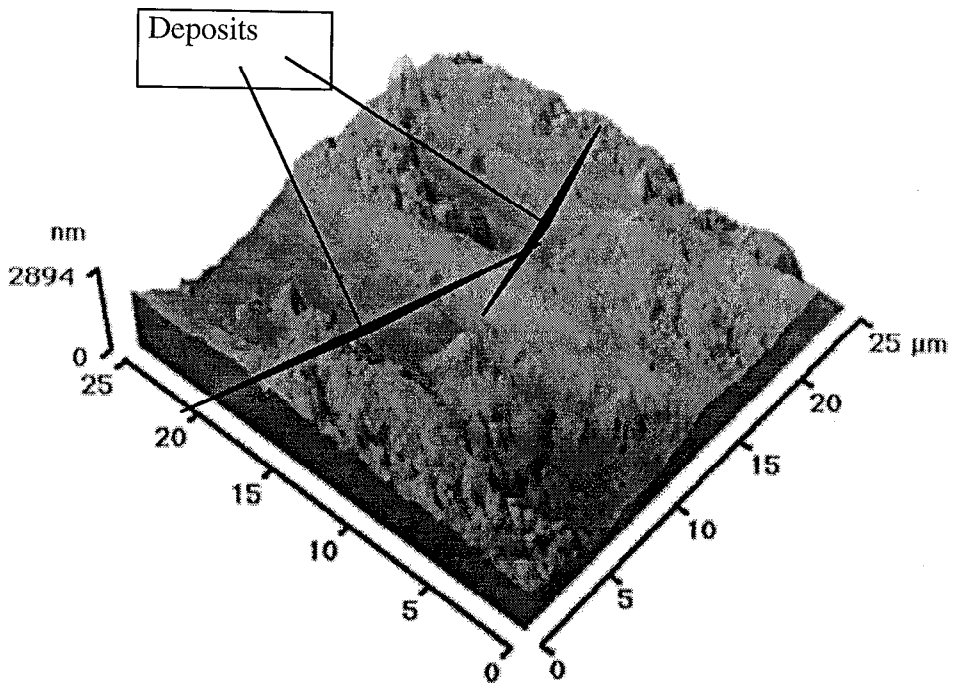

pb990607.054 AFM Image

SCW Test Coupons

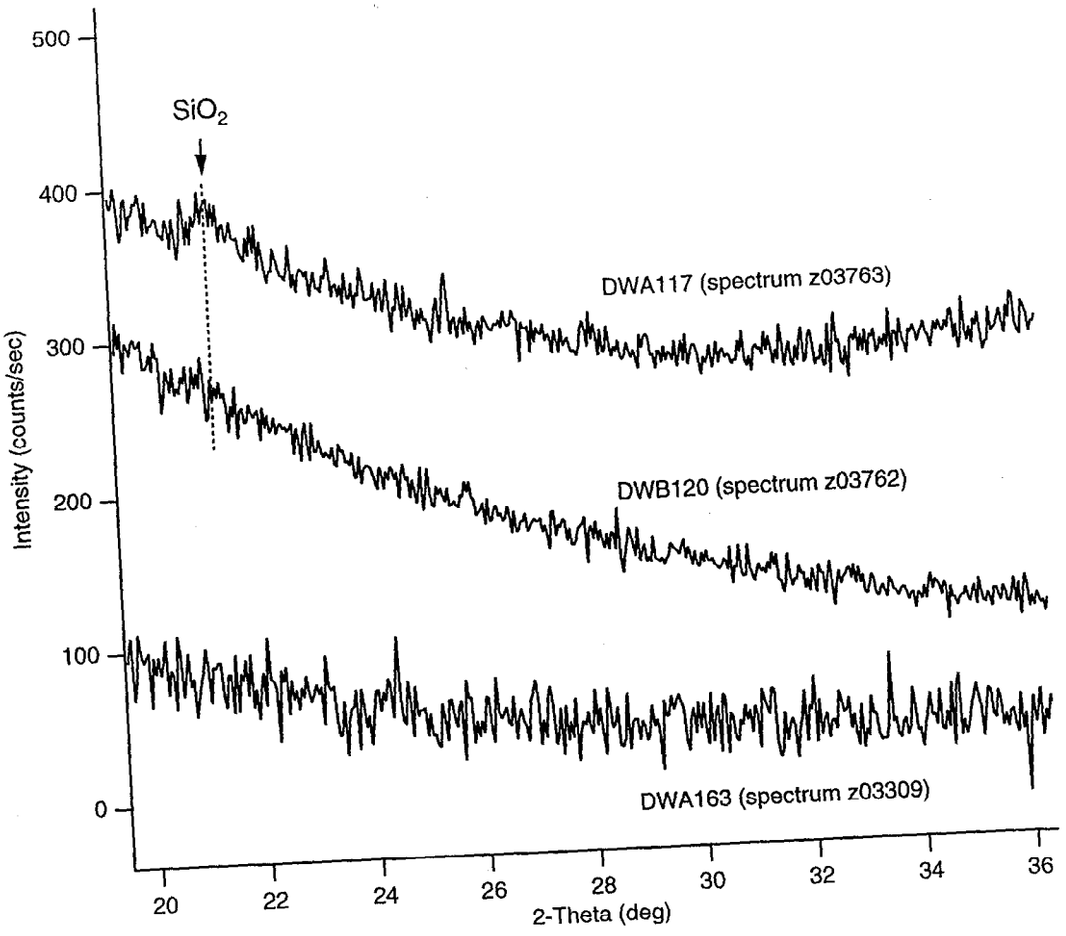

X-Ray Spectra of Scales on SCW Test Coupons

DWA 120 (SCW, 90C, Aqueous)

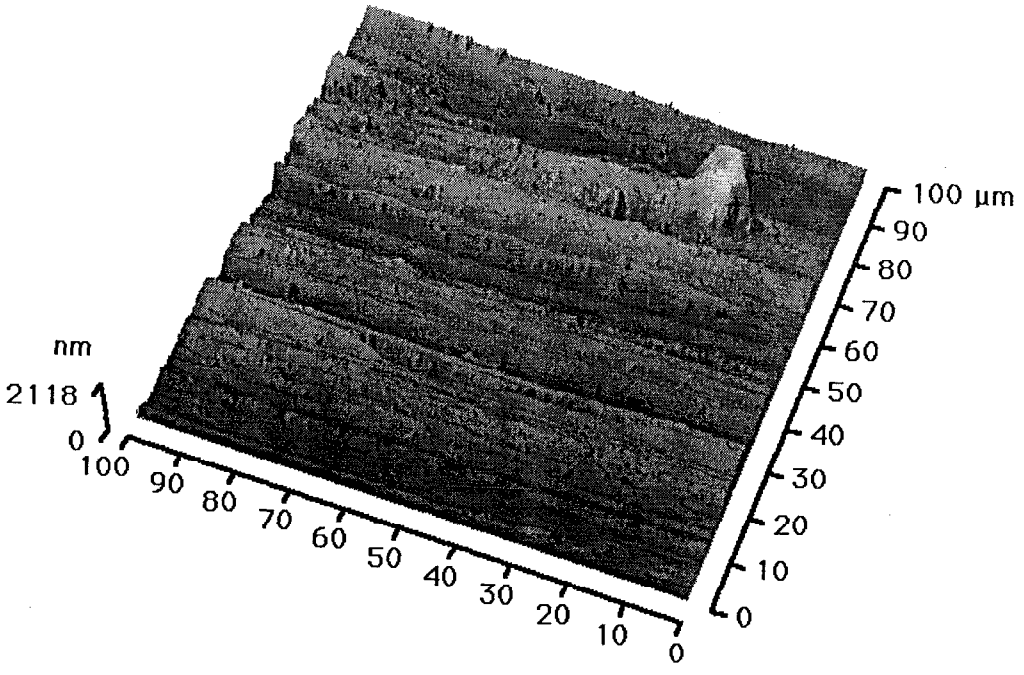

pb990607.001 AFM Image

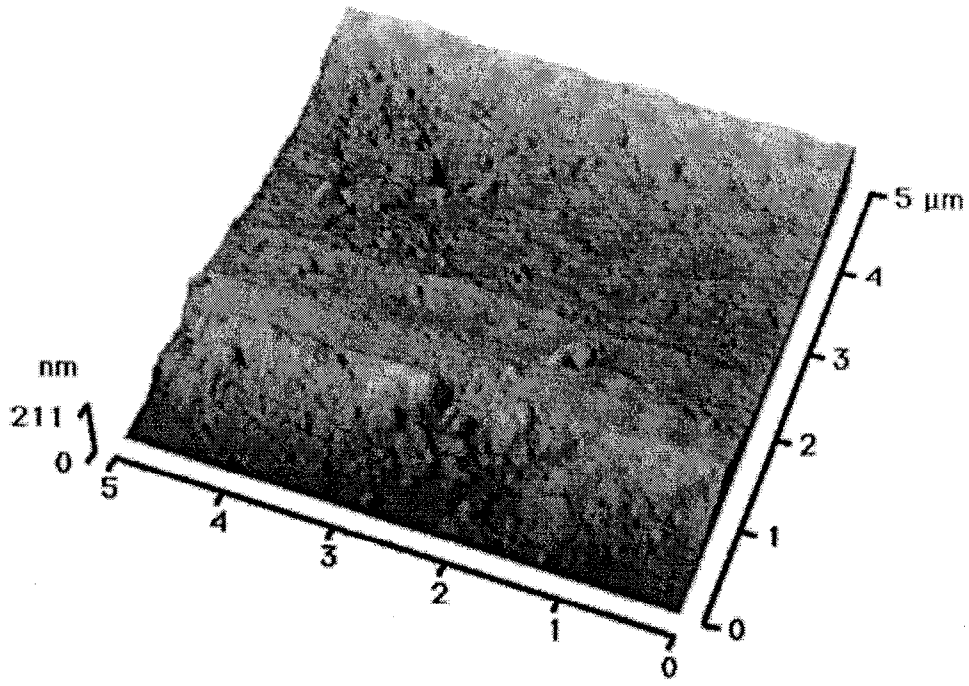

pb990607.005 AFM Image

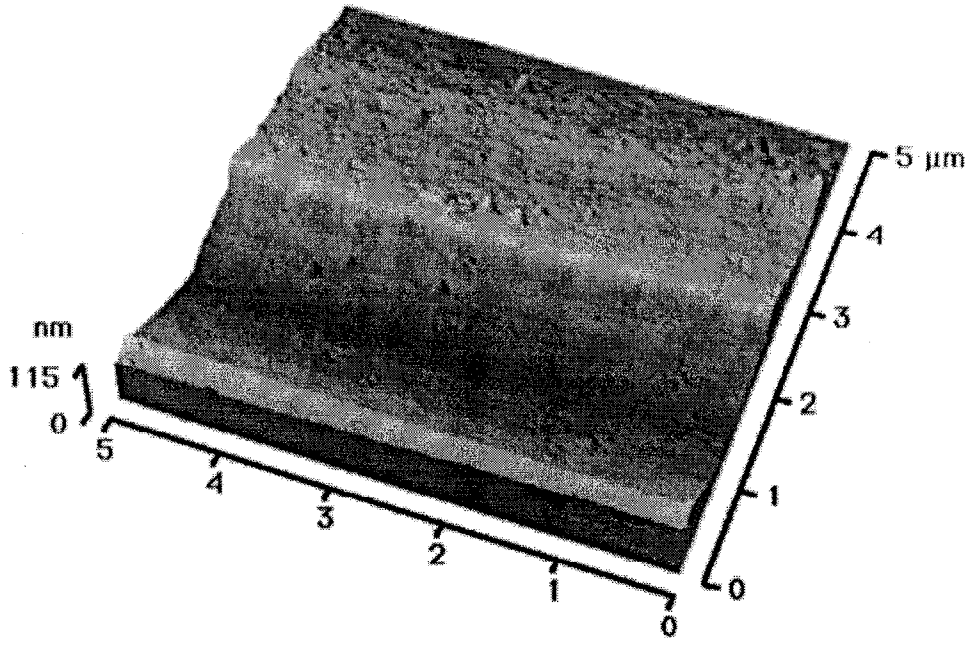

pb990607.015 AFM Image

DWA117 (SCW, 90C, Vapor)

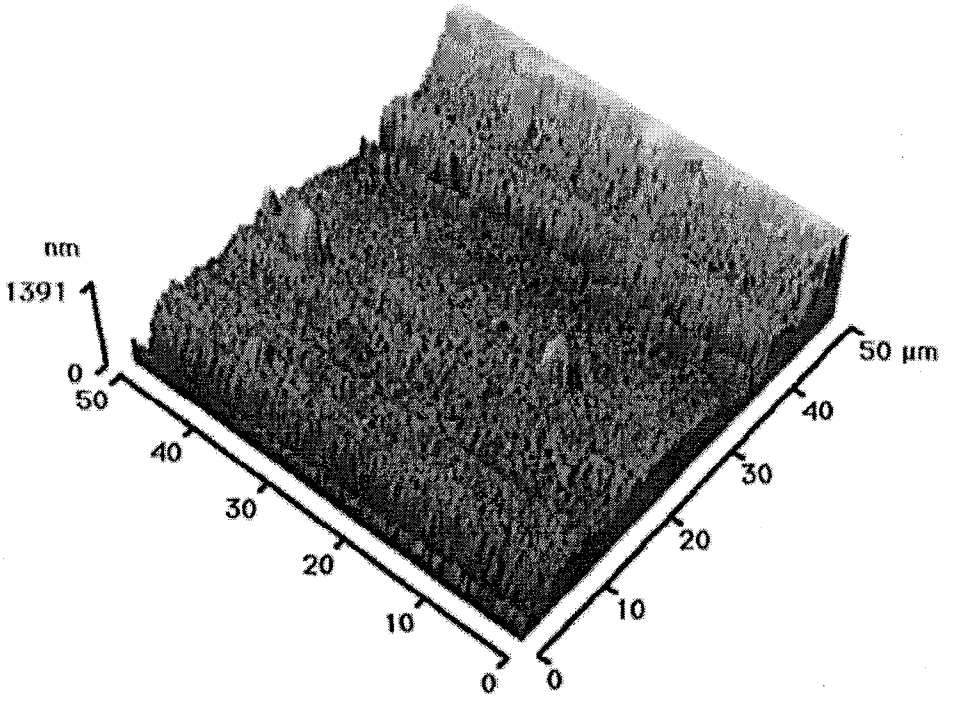

pb990607.039 AFM Image

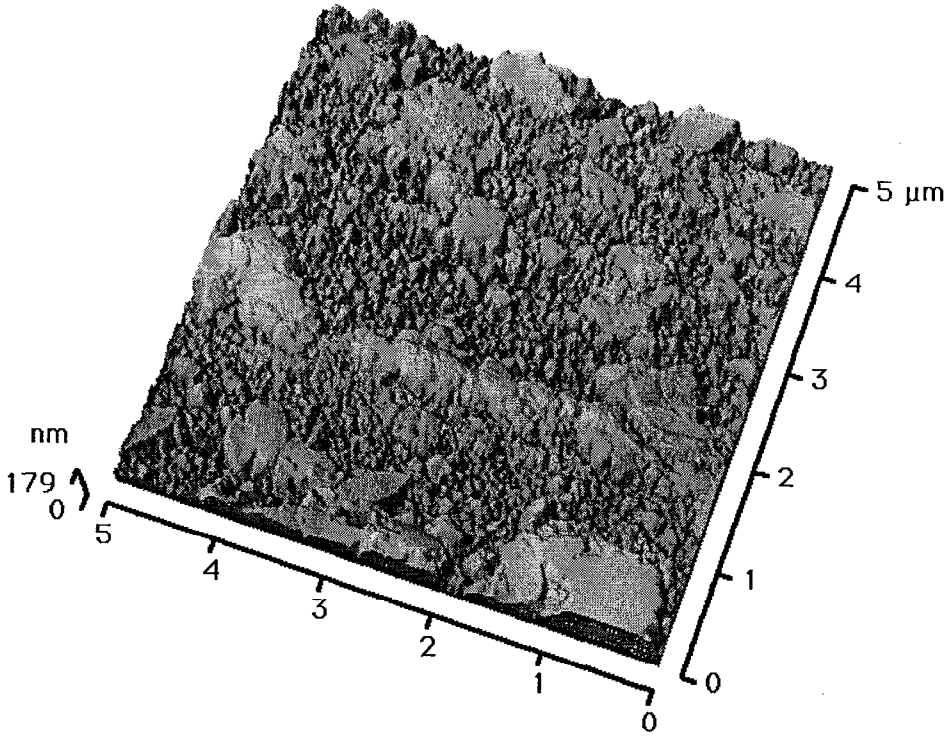

pb990607.035 AFM Image

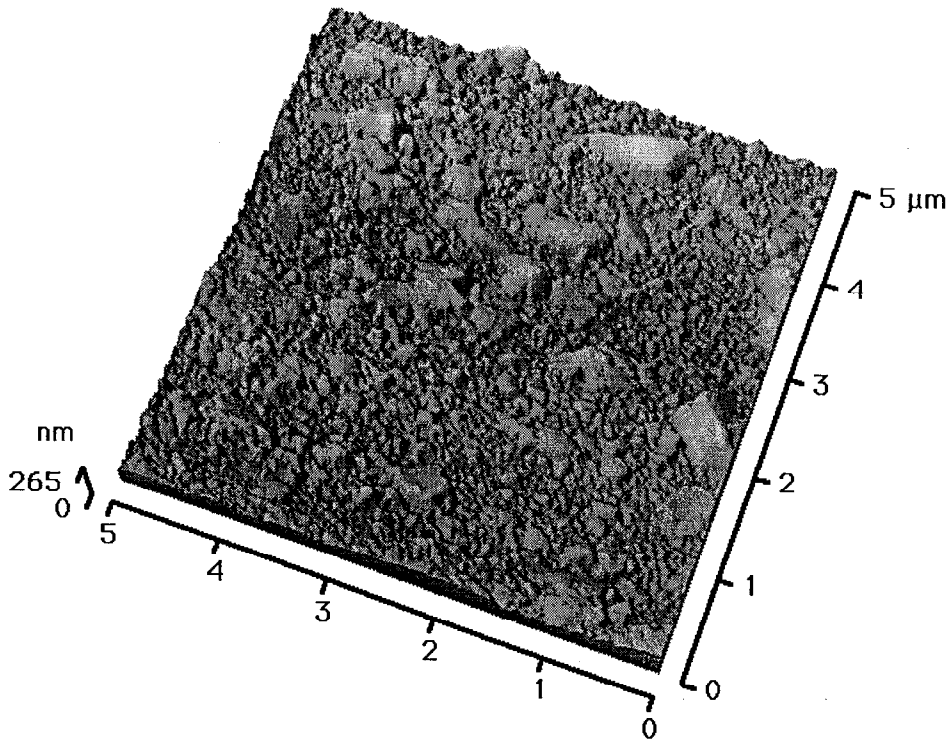

pb990607.037 AFM Image

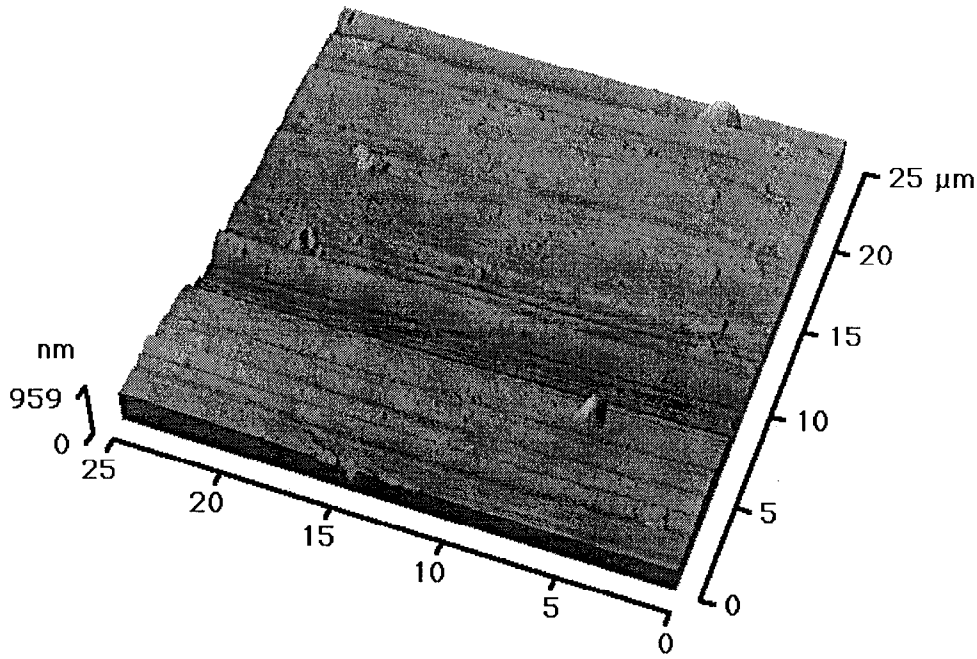

pb990607.044 AFM Image

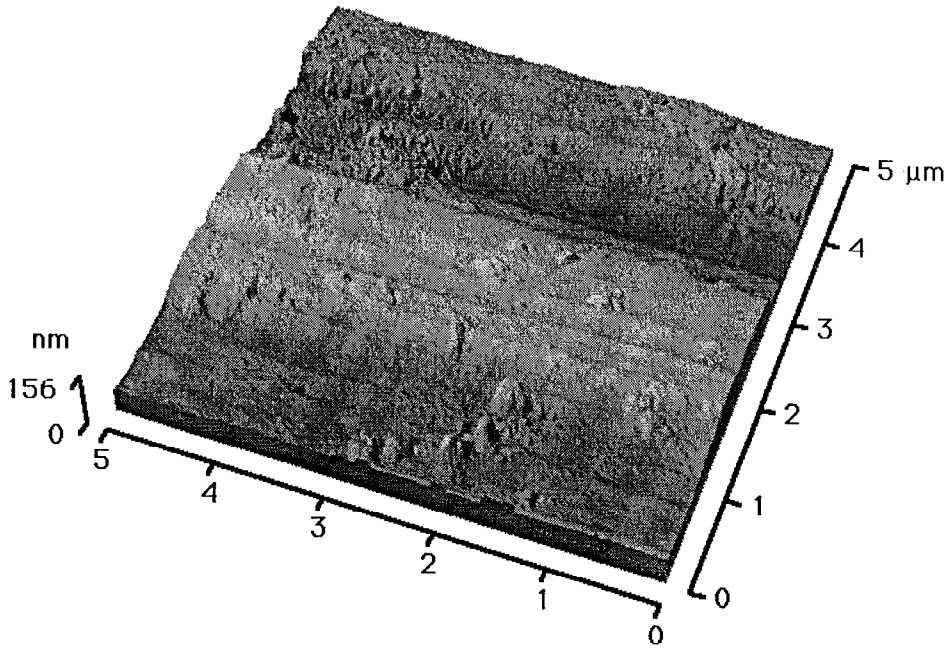

pb990607.041 AFM Image

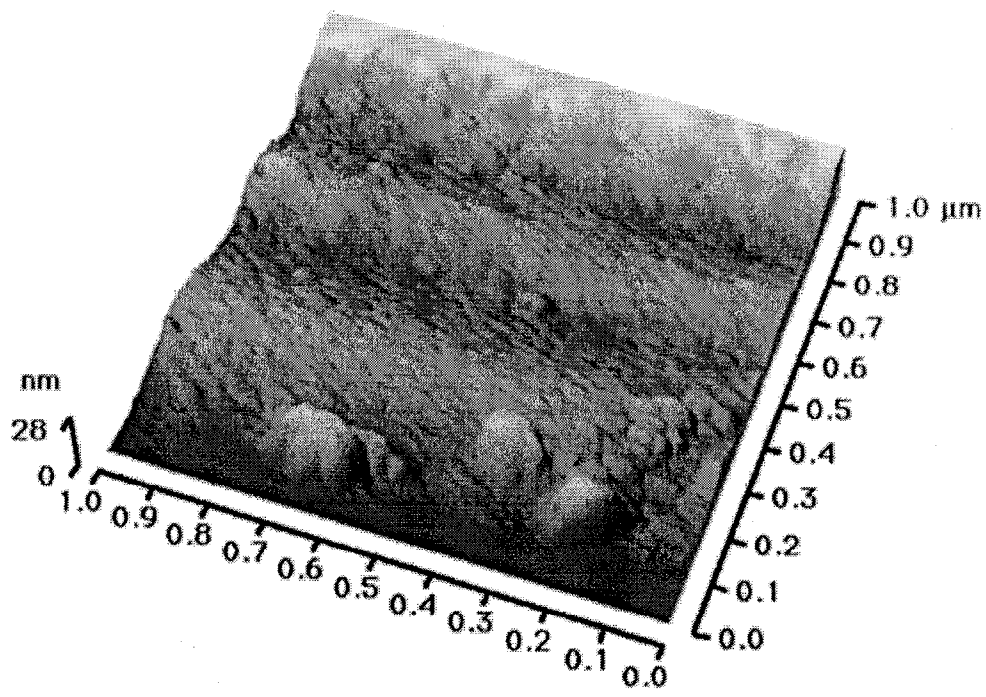

pb990607.042 AFM Image

Proposal No. 9954/2506M

X-RAY WAVEGUIDES FOR HIGH RESOLUTION X-RAY ANALYSIS

Troy W. Barbee, Jr.
Lawrence Livermore National Laboratory
Livermore CA 94550

Introduction

The ability to characterize crystallographic and compositional distributions in macroscopic material samples significant to DOE - relevant materials as well as a more general class of technologically important materials at sub-100-nm resolution levels is not possible with traditional x-ray technologies. This ability would offer the materials community new understanding of relationships among synthesis, structure, and property and would enable materials engineering at the mesoscopic-to-microscopic scales.

The project goals were to model, synthesize, and characterize thin-film, x-ray waveguide structures to determine whether such nanostructures can be fabricated with the precision required for true waveguide operation at x-ray energies. In FY98, we designed, fabricated, and characterized (at the Stanford Synchrotron Radiation Laboratory) optimized, thin-film, x-ray waveguide structures (XWGs) as resonant concentrators of x-rays which may be applied as diffraction-limited, linear x-ray sources. We fabricated nine waveguide structures that were optimized to operate in the cavity modes m = 1,2,3 and tested them at x-ray energies of 6 to 10 keV. The observed performances were compared to the calculations based on the design strucutres and excellent agreement was demonstrated.

The LLNL LDRD project contained tasks as presented in TABLE1. which include all aspects of the development of these unique thin film x-rtay optical devices. X-ray waveguide designs were made using a standard x-ray multilayer x-ray optic Fresnel code. Materials were selected on the basis of calculated performance as well as sputter deposition characteristics. Laboratory x-ray reflectivity measurements were made prior to the SSRL experimental run to assess the quality of the samples. Cross-section Transmission Electron Microscopy observations of selected sample were made to enable asssessment of the relationship between the design structures and the fabricated structures. The cross-section TEM observations corrrelated well with the waveguide fabricaiton parameters supporting the observed corrlations between the experimental and calculated grazing incidence reflectivities and fluorescence as functions of both x-ray energy and grazing angle of incidence.

TABLE 1.
LLNL X-ray Waveguide Project

A.X-ray Waveguide A Cavity Design/Model Calculations
1. As a function of Cavity Structure
2. As a function of Cavity Materials
3. As a function of Wavelength
4. As a function of Waveguide Mode

B.X-ray Waveguide Cavity Fabrication
1. Multilayer Synthesis process
2. Substrates
3. Preparation of the Cavity Termination Emitting Surface

C. X-ray Waveguide Cavity-Laboratory Characterization
1. X-ray Reflectivity/Fluorescence
    a. LLNL Laboratory
    b. Synchrotron
2. LLNL SEM/TEM Structural Characterization
    a. Plan View and Cross-Section View
    b. Interfacial Structure

D. Waveguide Performance-Synchrotron
1. As a function of Waveguide Structure
2. As a function of Waveguide Materials
3. As a function of Wavelength
4. As a function of Waveguide Mode
5. Comparison With Model Calculations